

Supporting Information

Molecular and Nano Structures of Chiral PEDOT Derivatives Influence the Enantiorecognition of Biomolecules. *In Silico* Analysis of Chiral Recognition

Jayakrishnan Aerathupalathu Janardhanan,^{a,b,c,d} Anusha Valaboju,^{b,e} Udesh Dhawan,^{a,b} Tharwat Hassan Mansoure,^{a,b} Ching-Cher Sanders Yan,^b Chou-Hsun Yang,^b Bhaskarchand Gautam,^{a,b} Chao-Ping Hsu^{*b,f} and Hsiao-hua Yu^{*a,b}

Table of Contents

1. Materials and Methods	S2
2. Synthetic route to (R) and (S)-EDOT-OH.	S3
3. Electropolymerization and Electrochemical Analysis of RP and SP.	S5
4. Characterization of Morphology and Surface Properties of Chiral Polymers.	S7
5. QCM Measurements.	S7
6. In Vitro Cytotoxicity Analysis	S9
6.1. Morphological Analysis Performed Using Immunocytochemistry	S10
6.2. Protein Secretion Observed Using Scanning Electron Microscopy (SEM)	S10
7. Computational Methods	S11
7.1 Additional Computational Results	S12
8. References	S21
9. NMR Spectra of the compounds	S22

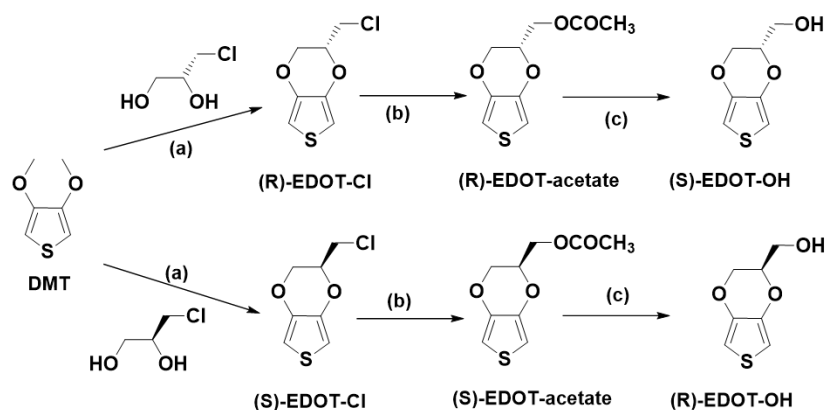
Experimental

Materials and Methods.

3,4-Dimethoxythiophene (95+%; Matrix Scientific), p-toluenesulfonic acid monohydrate (p-TSA, 99%; Alfa Aesar), (R)- and (S)-3-chloro-1,2-propanediol (ee 98%; Alfa Aesar), sodium acetate anhydrous (99%; Sigma–Aldrich), sodium hydroxide (98%; Sigma–Aldrich), tetrabutylammonium perchlorate (TBAP), and lithium perchlorate (99%; Alfa Aesar), sodium dodecyl sulphate (SDS, J. T. Baker) were used as received. Toluene (anhydrous, analytical grade; Macron Fine Chemicals) and dimethylsulfoxide (DMSO, HPLC grade; TEDIA High Purity Solvents) were purchased in sealed bottles. Solvents were added to reaction flasks under N₂ gas. Deuterated solvents were purchased from Sigma–Aldrich. ¹H and ¹³C nuclear magnetic resonance (NMR) spectra were acquired at 25°C using Bruker AVA-300 and AVIII-400 spectrometers. Chemical shifts are reported on the δ scale (ppm) with residual solvent peaks used as internal standards. UV–Vis spectra were recorded using a Cary 8454 UV–Vis spectrophotometer (Agilent Technologies). Fourier transform infrared (FTIR) spectra were recorded using a PerkinElmer FTIR instrument. Circular dichroism (CD) spectra were recorded using a JASCO-J 870 spectropolarimeter. Mass spectra (MS) were recorded using a time-of-flight (TOF) mass spectrometer. Specific optical rotations were measured using a JASCO-P2000 digital polarimeter. Phosphate-buffered saline (PBS) was used as a standard for the QCM studies. FBS (Gibco™; Fisher Scientific) was the model protein used in this study. RGD peptide was purchased from Mission Biotech and insulin (human recombinant) from Sigma–Aldrich. The enantiomers of MA (98% ee) were purchased from TCI Chemicals, Japan. Indium tin oxide (ITO)–coated glasses were cleaned by immersion in detergent solutions, acetone, CH₂Cl₂, MeOH, isopropyl alcohol, and then finally deionized water with ultrasonic agitation for a period of 30 min prior to use.

2. General procedure for synthesis of (R) and (S)-EDOT-OH.

Synthesis of these monomers was performed through transesterification of 3,4-dimethoxythiophene with (R)- and (S)-3-chloro-1,2-propanediol and two subsequent steps, as displayed in Scheme 1.



Scheme S1. Synthesis of (R)- and (S)-EDOT-OH. Conditions: (a) *p*-TSA, toluene, 90 °C; (b) sodium acetate, DMSO, 120 °C; (c) NaOH, H₂O.

2.1 Synthesis of (S)-Chloromethyl-EDOT [(S)-EDOT-Cl]

p-TSA (0.376 g, 2.00 mmol) was added to a two-necked round-bottom flask charged with a magnetic stirrer bar. After evacuating the flask and backfilling with N₂, 3,4-dimethoxythiophene (2.80 g, 20.0 mmol) was added followed by anhydrous toluene (40 mL). The solution was stirred for 5 min at room temperature and then (S)-3-chloro-1,2-propanediol (4.90 g, 44.3 mmol) was added. After heating the mixture at 90 °C for 48 h, a further charge of (S)-3-chloro-1,2-propanediol (4.90 g, 44.3 mmol) was added and then the mixture was stirred for 36 h. The mixture was cooled to room temperature and the solvent was evaporated. The tar-like residue was purified through column chromatography (SiO₂; hexane/EtOAc, 20:1) to provide a white solid (2.13 g, 56.2%).

(S)-EDOT-Cl: $[\alpha]_D^{23} = +2.65$ ($C = 1$; CHCl₃). ¹H NMR (400 MHz, CDCl₃, ppm) δ : 6.41 (d, $J = 5.2$ Hz, 1H), 6.38 (d, $J = 5.6$ Hz, 1H), 4.44–4.37 (m, 2H), 4.34–4.29 (m, 1H), 3.79–3.67 (m, 2H). ¹³C NMR (100 MHz, CDCl₃, ppm) δ : 141.17, 140.71, 100.18, 72.89, 65.61, 41.37. HRMS (EI⁺): $[M^+]$ calcd for C₇H₇ClO₂S, m/z 189.9855; found, 189.9855.

2.2 Synthesis of (S)-EDOT-acetate

A 250-mL round-bottom flask was charged with a stirrer bar, (S)-EDOT-Cl (2.10 g, 11.1 mmol), and anhydrous sodium acetate (1.36 g, 16.7 mmol) and then the backfilled three times with N₂. DMSO (50 mL) was added and the solution stirred at 120 °C for 24 h. Thin layer chromatography (TLC) confirmed that the reaction was complete. The mixture was cooled to room temperature, poured into water (40 mL), and extracted with CH₂Cl₂. The combined organic phases were dried (MgSO₄) and concentrated. The residue was purified through column chromatography (SiO₂; hexane/EtOAc, 8.5:1.5) to give a white solid (2.05 g, 86.5%).

(S)-EDOT-acetate: $[\alpha]_{\text{D}}^{23} = +30.8$ ($C = 1$; CHCl₃). ¹H NMR (400 MHz, CDCl₃, ppm) δ : 6.40 (d, $J = 4.8$ Hz, 1H), 6.38 (d, $J = 5.2$ Hz, 1H), 4.44–4.38 (m, 2H), 4.34–4.30 (m, 2H), 4.14–4.04 (m, 1H), 2.14 (s, 3H). ¹³C NMR (100 MHz, CDCl₃, ppm) δ : 170.62, 141.21, 141.04, 100.12, 99.99, 71.47, 65.61, 62.38, 20.74. HRMS (EI+): $[M^+]$ calcd for C₉H₁₀O₄S, m/z 214.0300; found, 214.0302.

2.3 Synthesis of (R)-EDOT-OH

A solution of NaOH (1.37 g, 34.3 mmol) in water (40 mL) was added to a round-bottom flask equipped with a reflux condenser. A solution of (S)-EDOT-acetate (2.00 g, 9.33 mmol) in THF (20 mL) was added and then the mixture was heated under reflux for 3 h while monitoring through TLC. The mixture was cooled to room temperature. Water (20 mL) was added and the pH adjusted to neutral with 1 M HCl. The aqueous phase was extracted three times with CH₂Cl₂. The combined organic phases were concentrated (rotary evaporator) and purified through column chromatography (SiO₂; hexane/EtOAc, 8:2) to give a colorless oil (1.52 g, 93.4%) that turned solid upon storage at –20 °C.

(R)-EDOT (OH): $[\alpha]_{\text{D}}^{23} = +21.8$ ($C = 1$; CHCl₃). ¹H NMR (400 MHz, CDCl₃, ppm) δ : 6.31 (s, 2H), 4.24–4.17 (m, 2H), 4.09–4.02 (m, 1H), 3.86–3.75 (m, 2H), 2.44 (br, 1H). ¹³C NMR (100 MHz, CDCl₃, ppm) δ : 141.40, 99.87, 74.08, 65.73, 61.52. HRMS (EI+): $[M^+]$ calcd for C₇H₈O₃S, m/z 172.0194; found, 172.0197.

2.4 Synthesis of (R)-Chloromethyl-EDOT [(R)-EDOT-Cl]

Obtained as a white solid (1.95 g, 52.8%) from (R)-3-chloro-1,2-propanediol through the procedure described above for (S)-EDOT-Cl.

(R)-EDOT-Cl: $[\alpha]_D^{23} = -2.7$ ($C = 1$; CHCl_3). ^1H NMR (400 MHz, CDCl_3 , ppm) δ : 6.35 (d, $J = 4$ Hz, 1H), 6.33 (d, $J = 4$ Hz, 1H), 4.38–4.27 (m, 2H), 4.23–4.09 (m, 1H), 3.73–3.61 (m, 2H); ^{13}C NMR (100 MHz, CDCl_3 , ppm) δ : 141.17, 140.72, 100.18, 72.89, 65.61, 41.36. HRMS (EI+): $[\text{M}^+]$ calcd for $\text{C}_7\text{H}_7\text{ClO}_2\text{S}$, m/z 189.9855; found, 189.9852.

2.5 Synthesis of (R)-EDOT-acetate

Obtained as a white solid (1.70 g, 84.1%) from (R)-EDOT-Cl (1.80 g, 9.44 mmol) and anhydrous sodium acetate (1.10 g, 13.4 mmol) through the procedure described above for (S)-EDOT-acetate.

(R)-EDOT-acetate: $[\alpha]_D^{23} = -30.5$ ($C = 1$; CHCl_3). ^1H NMR (400 MHz, CDCl_3 , ppm) δ : 6.35 (d, $J = 4.8$ Hz, 1H), 6.33 (d, $J = 4.8$ Hz, 1H), 4.39–4.35 (m, 2H), 4.34–4.27 (m, 1H), 4.05–3.98 (m, 2H), 2.09 (s, 3 H). ^{13}C NMR (100 MHz, CDCl_3 , ppm) δ : 170.61, 141.20, 141.03, 100.12, 99.99, 71.47, 65.61, 62.38, 20.74. HRMS (EI+): $[\text{M}^+]$ calcd for $\text{C}_9\text{H}_{10}\text{O}_4\text{S}$, m/z 214.0300; found, 214.0300.

2.6 Synthesis of (S)-EDOT-OH

Obtained as a colorless oil (1.20 g, 90.4%), which turned solid upon storage at -20 °C, from (R)-EDOT-acetate (1.65 g, 7.71 mmol) and NaOH (1.37 g, 34.3 mmol) through the procedure described above for (R)-EDOT-OH.

(S)-EDOT-OH: $[\alpha]_D^{23} = -22.1$ ($C = 1$; CHCl_3). ^1H NMR (400 MHz, CDCl_3 , ppm) δ : 6.37 (s, 2H), 4.48–4.23 (m, 2H), 4.15–4.08 (m, 1H), 4.02–3.62 (m, 2H), 2.46 (br, 1H). ^{13}C NMR (100 MHz, CDCl_3 , ppm) δ : 141.41, 99.86, 74.04, 65.74, 61.60. HRMS (EI+): $[\text{M}^+]$ calcd for $\text{C}_7\text{H}_8\text{O}_3\text{S}$, m/z 172.0194; found, 172.0197.

3. Electropolymerization and Electrochemical Analysis of RP and SP.

The electrochemical polymerization was performed using a potentiostat (PGSTAT128N, Autolab) in a typical three-electrode system at room temperature (23 ± 2) °C. An ITO-coated glass electrode or a Au chip for QCM experiments was used as the working electrode;

Ag/AgCl and Ag/Ag⁺ electrodes were used as reference electrodes in aqueous and organic solutions, respectively; Pt wire was used as the counter-electrode. All monomer solutions were deaerated under a flow of N₂ prior to the electropolymerization to avoid any effects of O₂. Nanotubular RP and SP films were prepared by dissolving the (S)- or (R)-EDOT-OH monomer (10 mM) in CH₂Cl₂ containing 100 mM TBAP and then applying a constant potential of +1.2 V (vs Ag/Ag⁺) for 60 s at room temperature. Smooth thin films were fabricated on the electrode surface from an aqueous solution of 10 mM (R)- or (S)-EDOT-OH, 100 mM LiClO₄, and 50 mM sodium dodecyl sulfate (SDS) by applying a constant potential of +1.2 V (vs Ag/AgCl) for 60 s at room temperature. The deposition of RP and SP on the electrode surfaces were confirmed by cyclic voltammetry. The resulting polymer films were washed thoroughly with MeCN and doubly distilled deionized water to remove the supporting electrolyte and any non-polymerized monomer.

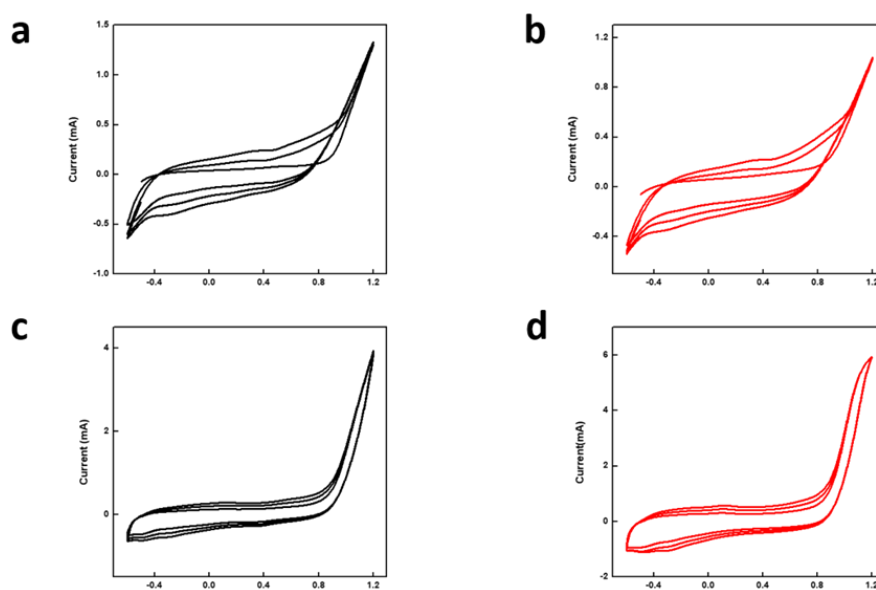


Figure S1. Electropolymerization curves of (R)- and (S)-EDOT-OH recorded while applying cyclic potential (CV) to Au-coated QCM sensor chips. SP- and RP-nanotube structures were formed (Fig. a, b respectively) when applying a cyclic potential ranging from -0.6 to $+1.2$ V (vs Ag/Ag⁺) for three cycles in CH₂Cl₂ with TBAP as the supporting electrolyte at room temperature (Fig. a, b respectively). SP- and RP-smooth film structures were formed when applying a cyclic potential ranging from -0.6 to $+1.2$ V (vs Ag/AgCl) for three cycles in aqueous LiClO₄ with SDS at room temperature Scanning rate: 100 mV/s. (Fig. c, d respectively).

4. Characterization of Morphology and Surface Properties of Chiral Polymers.

The surface morphologies of the RP and SP materials were investigated using a Zeiss-Ultra Plus field emission scanning electron microscope operated at an accelerating voltage of 10 kV and a working distance of 10 mm. FTIR, UV–Vis, and CD spectra were recorded to characterize the chiral polymer materials. DMSO was used as the solvent for the UV–Vis and CD spectroscopic experiments. For de-doping, a few drops of hydrazine hydrate were added to the polymer solution and then the mixture was left for 1 h. An OCA contact angle system was used for measurement of water contact angles. Water droplets were placed on the surface and then the contact angles were measured using the SCA20 software of the OCA system. Experiments were repeated at least three times for each polymer.

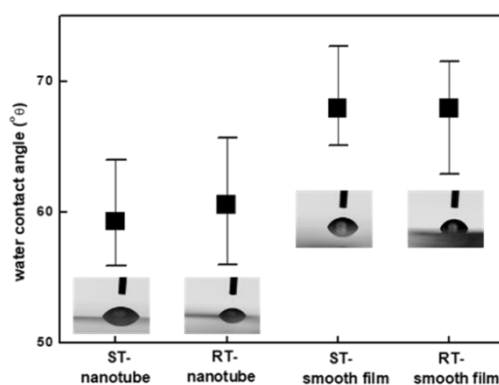


Figure S2. Results of water contact angle measurements.

5. QCM Measurements.

QCM experiments were conducted using a Q-Sense E4 system (Biolin Scientific AB, QE401-F1521, Finland). Prior to the electropolymerization process, Au-coated QCM sensor crystals were cleaned using piranha solution for use as the working electrode. (R)- and (S)-EDOT-OH were electropolymerized directly on Au-coated crystals having a diameter of 14 mm. QCM measurements were conducted at a fundamental frequency of 4.95 MHz. Solutions were pumped using a microprocessor-controlled dispensing pump (IPC-4, Ismatec) at a flow rate of 50 $\mu\text{L}/\text{min}$ at 25 $^{\circ}\text{C}$. All QCM experiments were repeated a minimum of three times. The Au-coated QCM sensors presenting the RP and SP materials were installed in the chamber; PBS buffer (1x, pH 7.2) was passed through the chamber to stabilize the fundamental frequency and overtones. Once equilibrium had been reached, solutions of various

bioanalytes in PBS buffer (1 mg/mL) were pumped through the system for 30 min. After adsorption of the bioanalytes, PBS buffer was again passed through the system to rinse the sensor surface. The shift in frequency was recorded directly using QSoft 401 software. The frequency readout was converted into a mass change by using the Sauerbrey equation

$\Delta m = -C\Delta f/n$, where Δf is the frequency change, C is a constant, n is the overtone, and Δm is the mass change (Table S1).

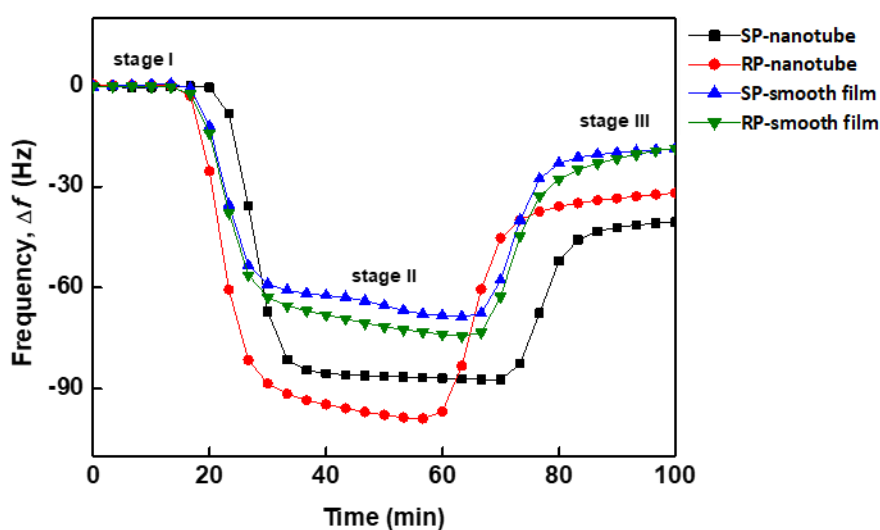


Figure S3. QCM frequency readouts for FBS protein on RP-nanotube, SP-nanotube, RP-smooth film, and SP-smooth film structures.

	SP-nanotube		RP-nanotube		SP-Smooth film		RP-smooth film	
	ΔF (Hz) ^a	$M(\text{ng}/\text{cm}^2)$ ^b						
FBS Protein	40.7	240.13	34.13	201.38	20.36	120.12	20.03	118.21
Selectivity ratio (SP/RP)^c	1.19				1.02			
RGD Peptide	8.59	50.68	5.75	33.92	3.46	20.45	2.91	17.16
Selectivity ratio (SP/RP)^c	1.49				1.18			

Insulin	7.87	46.46	10.36	61.12	0.885	5.22	0.93	5.48
Selectivity ratio (SP/RP)^c		1.31				1.05		
R-MA	10.21	60.25	5.92	34.94	1.31	7.72	1.16	6.88
Selectivity ratio (SP/RP)^c		1.72				1.12		
S-MA	6.3	37.17	10.67	62.95	1.15	6.80	1.67	9.9
Selectivity ratio (SP/RP)^c		1.69				1.45		
Selectivity ratio (R-MA/S-MA)^d	1.62		1.80		1.13		1.43	

^a Average values of change in QCM frequency readout.

^b Mass of analyte deposited, calculated using the Saurbrey equation.

^c Chiral selectivity ratio calculated by considering the QCM frequency readout or mass deposited on the RP- and SP-nanotube or RP- and SP-smooth film structures.

^d Chiral selectivity ratio calculated by considering the frequency readout or mass deposited by (R)- and (S)-MA on the RP-nanotube, SP-nanotube, RP-smooth film, and SP-smooth film structures.

Table S1. QCM frequency readouts and corresponding mass deposited by FBS, RGD, Insulin and R-MA and S-MA on RP/SP nanotubes and smooth films

6. *In Vitro* Cytotoxicity Analysis

The *in vitro* cytotoxicity of MCF-7 cells on the chiral smooth film and nanostructured materials was evaluated using an MTT assay. The MTT reagent was prepared by following the manufacturer's instructions. Cells were seeded on the substrates at a density of 2000 cells/cm² for 5 days in a six-well culture dish. After a predetermined time period, the medium was aspirated and the cells were washed three times with PBS, followed by incubation in MTT reagent. The cells were incubated at 37 °C for 4 h and then the medium

was carefully aspirated without disturbing the purple crystals. The crystals were dissolved in DMSO (2 mL) and placed on an orbital shaker for 15 min at room temperature. The absorbance was measured using an ELISA reader (OD: 570 nm). Cells cultured on plain ITO substrates were used as a control.

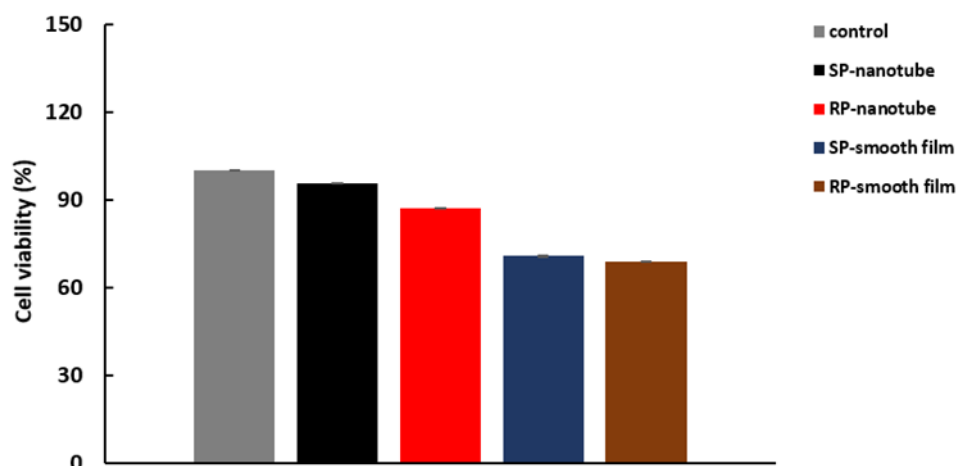


Figure S4. Results of cell viability tests

6.1. Morphological Analysis Performed Using Immunocytochemistry

F-actin filaments were stained to evaluate the modulation of cell morphology induced by the chiral smooth films and nanostructured materials. MCF-7 cells were seeded at a density of 2000 cells/cm² on the substrates in a six-well dish and left to grow for 5 days. After a predetermined time period, the cells were washed three times using pre-warmed PBS, followed by fixation in 4% formaldehyde for 10 min at room temperature. The cells were then washed three times with PBS and permeabilized by incubating in 0.1% Triton X-100 for 10 min at room temperature. The cells were then washed three times with PBS and incubated with 2% bovine serum albumin (BSA) for 1 h at room temperature, followed by incubation in FITC-phalloidin for 20 min. Finally, the cells were washed three times and mounted on a glass slide using ProLong Diamond antifade mounting medium with Dapi. The cells were imaged at 40x magnification using a Nikon Eclipse Ni-E fluorescent microscope.

6.2. Protein Secretion Observed Using Scanning Electron Microscopy (SEM)

To evaluate the cell morphology and to assess the degree of protein secretion, MCF-7 cells were seeded on the chiral smooth films and nanostructured materials. The cells were

seeded at a density of 2000 cells/cm² and left for 5 days. After a predetermined time period, the cells were washed with pre-warmed PBS and fixed in 3% glutaraldehyde for 30 min at room temperature. The cells were then washed three times with PBS and stained with OsO₄ for 30 min at room temperature. The cells were then incubated in 40% EtOH at 4 °C overnight. The next day, sequential dehydration was performed by incubating the cells in EtOH at varying concentrations (50, 60, 70, 75, 80, 85, 90, 95, and 100%) for 5 min each. Critical point drying was performed by incubating the cells in hexamethyldisilazane (HMDS) for 30 min. Samples were sputter-coated with Au and imaged using field emission scanning electron microscopy (FESEM; Zeiss-Ultra plus field emission scanning electron microscope).

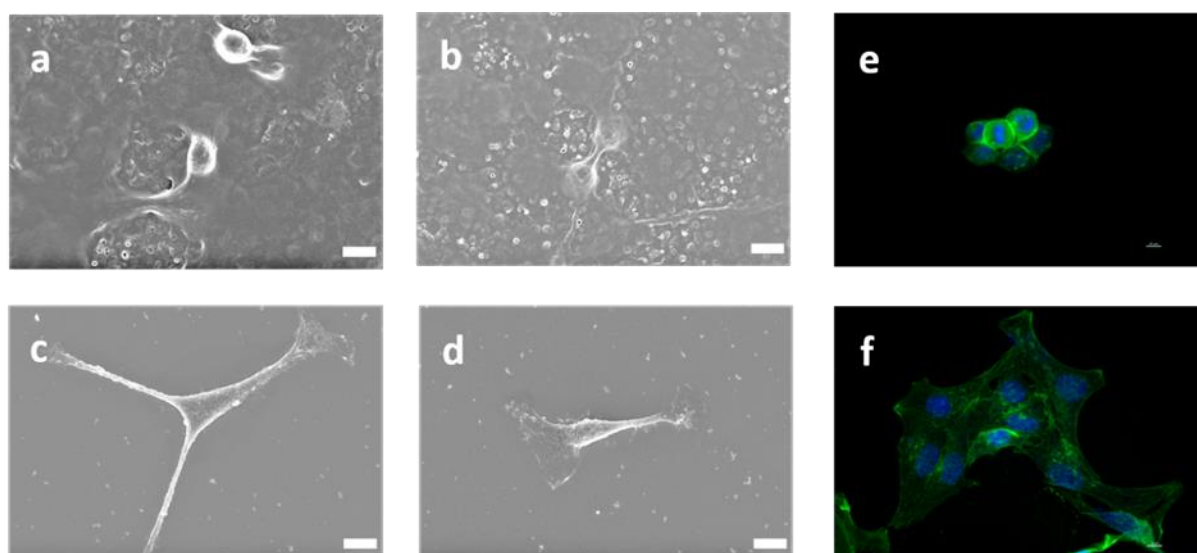


Figure S5. (a–d) SEM images of MCF-7 cells on (a) SP- and (b) RP-nanotube and (c) SP- and (d) RP-smooth film structures. (e, f) Immunofluorescence staining of the MCF-7 cytoskeleton, highlighting morphological control exerted by (e) nanotube and (f) smooth film structures. Scale bars: 10 μ M.

7. Computational Methods

A pair of spatially separated dimers were built for (R)-poly(EDOT-OH) with (R)- or (S)-MA, referred to as RPRM and RPSM, respectively, hereafter. A trimer of EDOT-OH was considered as a minimal PEDOT-OH unit. The binding pair was first formed by keeping equal the centroid–centroid distance between (R)-poly(EDOT-OH) and the two forms of MA. A first AIMD simulation was performed via Born–Oppenheimer propagation to search for

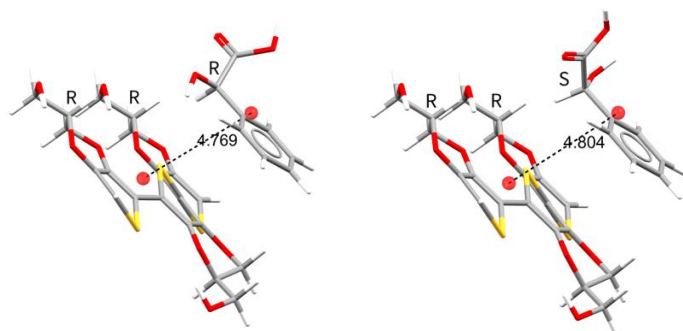
minimum-energy structures. The 50 lowest-energy structures were selected; among them, 9 unique structures were obtained for RPRM and 12 for RPSM—they were further optimized with DFT calculations and the results were used for further analysis in their interactions. The lowest-energy geometries of the two systems were picked as initial structures for three rounds of AIMD in a canonical NVT ensemble to model possible conformational fluctuations at room temperature.

Ground state geometry optimizations and AIMD simulations were performed using Q-Chem 5.2¹ software. The dispersion-corrected ω B97x-D3² functional and a 6-31G(d) basis set were used. Basis-set superposition error correction (BSSE) was employed for calculation of binding energies. For the AIMD simulations, the initial nuclear velocities were specified from a Maxwell–Boltzmann distribution at a given temperature of 298 K. The system was simulated for 5000 steps of 0.484 fs (20 a.u.) each. The simulations of the NVT ensemble at 298 K were performed using a Langevin thermostat with friction strength of 0.01 fs⁻¹. In all cases, the first 500 steps were disregarded in the analyses.

7.1 Additional Computational Results

To investigate the interactions of the various stereoisomers of EDOT-OH and the chiral mandelic acid (MA), we first formed a pair of similar conformations (Fig. S6) from which we began preliminary AIMD calculations for sampling of possible interacting structures. From the AIMD trajectories, we took the lowest-energy structures and obtained nine unique optimized structures for RPRM and 12 for RPSM.^a Further structural parameters, in addition to those in Table 1 of the main text, are listed here in Table S2. Structural characterization data are included in Fig. S7. All of the structures, with XYZ coordinates, are also included in a separate zipped file.³

^aRPRM6 was obtained with a slightly modified input geometry from the AIMD snapshot for full convergence in geometry optimization.



RPRM

RPSM

Fig. S6. Initial geometries of a trimer of EDOT-OH interacting with (*R*)- [or (*S*)-]MA, forming RPRM (RPSM) systems, which were used for initial AIMD simulations to search for low-energy interacting conformations. Stereocenters and centroid–centroid distances (Å) between the EDOT-OH trimer and MA are indicated.

Table S2. Additional structural parameters for the optimized structures.

	Distance (Å)										
	RPRM1										
O···H ^{a,b}	1.853	2.416	2.468	2.622	2.769	2.808	3.850				
OH···π ^c	2.943										
CH···π ^c	2.911	2.925	3.022	3.746	3.915						
	RPRM2										
O···H	1.795	1.888	2.821	2.822	3.055	3.031	3.138	3.703	3.957		
OH···π											
CH···π	2.873	3.621									
	RPRM3										
O···H	1.860	2.417	2.471	2.616	2.806	2.867	2.994	3.351	3.385	3.842	
OH···π	2.910										
CH···π	2.902	2.937	3.695	3.887							
	RPRM4										
O···H	2.34	2.349	2.594	2.731	2.74	3.017	3.314	3.429	3.466	3.573	3.734
OH···π	2.675										
CH···π	3.248	3.264	3.275								

RPRM5

O···H	2.338	2.382	2.654	2.705	2.735	2.748	3.028	3.197	3.279	3.413
OH··· π	2.645									
CH··· π	3.225	3.350								

RPRM6

O···H	2.010	2.764	2.803	2.826	2.979	3.316	3.479	3.790	3.822
OH··· π									
CH··· π	2.894	3.584							

RPRM7

O···H	1.844	2.468	2.469	2.57	2.764	2.828	2.967	3.396	3.671
OH··· π	2.875								
CH··· π	2.901	3.031	3.046	3.869	4.061				

RPRM8

O···H	2.343	2.369	2.636	2.716	2.735	3.062	3.229	3.319	3.404	3.727
OH··· π	2.638									
CH··· π	3.242	3.297	3.311							

RPRM9

O···H	2.339	2.347	2.576	2.744	3.059	3.196	3.320	3.448	3.756
OH··· π	2.69								
CH··· π	3.252	3.222	3.428						

RPSM1

O···H	2.337	2.482	2.498	2.671	2.988	3.182	3.641	3.694	3.721
OH··· π									
CH··· π	3.465	3.546	3.881						

RPSM2

O···H	1.888	2.316	2.493	2.809	2.922	3.718	3.758		
OH··· π									
CH··· π	3.637	3.290	3.756	4.086					

RPSM3

O···H	1.813	2.510	2.657	2.694	2.906	3.140	3.524		
-------	-------	-------	-------	-------	-------	-------	-------	--	--

OH··· π

CH··· π 3.253 3.460 3.530 4.039

RPSM4

O···H 1.997 2.307 2.694 3.114 3.420 3.598

OH··· π

CH··· π 2.367 2.531

RPSM5

O···H 1.832 2.289 2.64 2.645 2.693 2.894 2.976 3.062 3.019 3.435 3.911

OH··· π 3.613

CH··· π 2.728 2.746 3.246 3.471

RPSM6

O···H 2.291 2.348 2.641 2.865 3.263 3.329 3.602

OH··· π

CH··· π 3.649 3.765 3.859

RPSM7

O···H 1.932 2.554 2.611 2.691 3.070 3.308 3.347 3.410 3.774

OH··· π

CH··· π 2.600 3.297 3.860

RPSM8

O···H 1.851 2.326 2.481 2.717 2.812 2.829 2.887 3.611

OH··· π 3.595

CH··· π 2.651 2.802 3.416

RPSM9

O···H 1.850 2.330 2.472 2.709 2.832 2.836

OH··· π 3.594

CH··· π 2.663 2.799 3.418

RPSM10

O···H 1.886 2.322 2.459 2.783 2.962 3.786

OH··· π

CH··· π

RPSM11

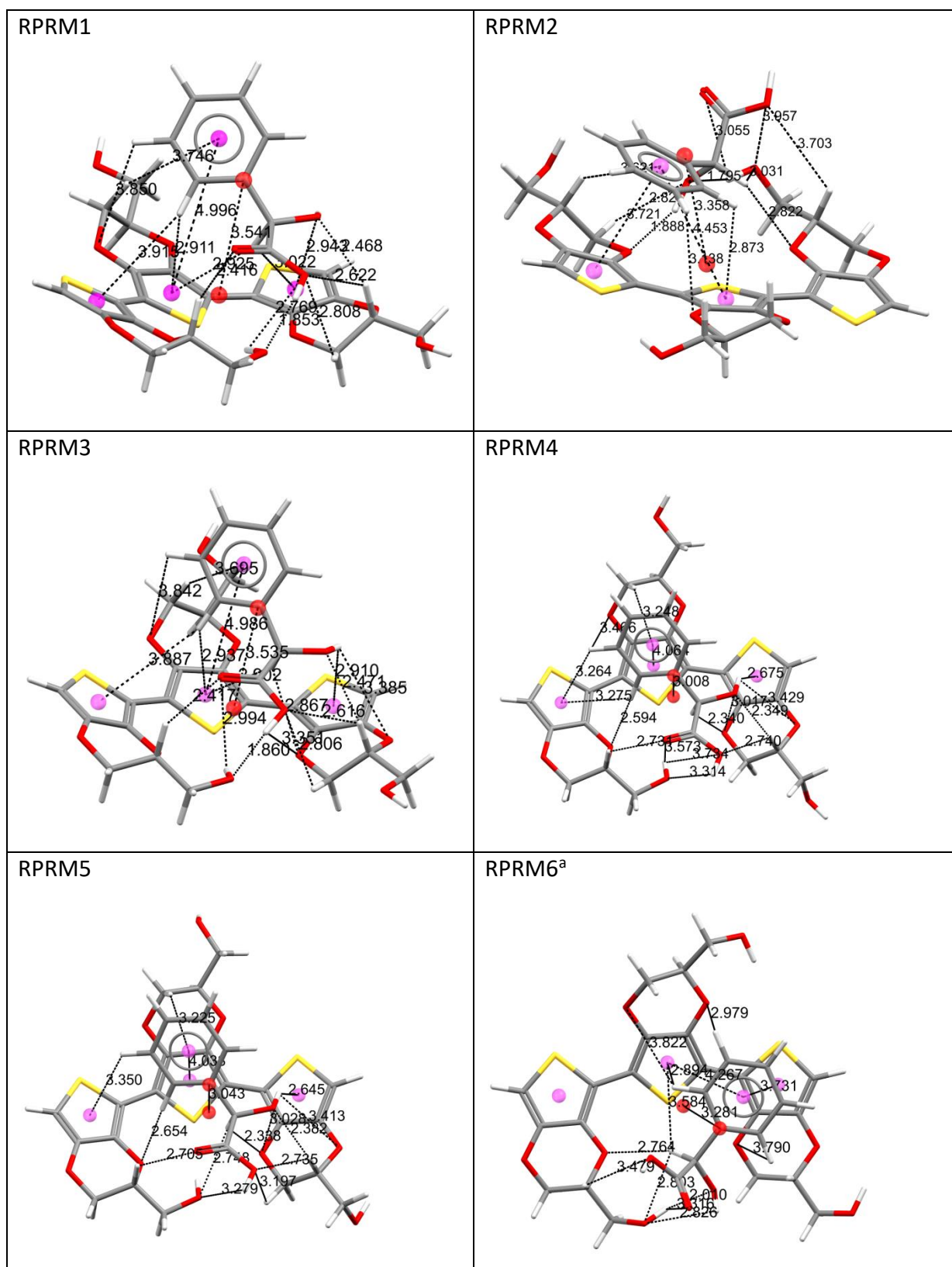
O···H	1.888	2.313	2.482	2.796	2.925	3.685	3.687	3.706	3.731
OH··· π									
CH··· π	3.282	3.650							

RPSM12

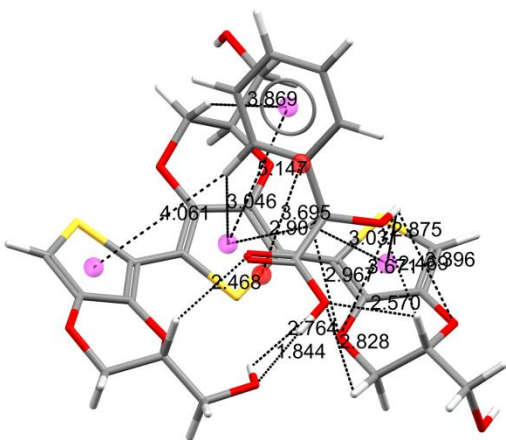
O···H	2.093	2.338	2.429	2.984	3.519	3.773	3.886		
OH··· π									
CH··· π	2.753	3.805	3.879						

- Red-shaded data indicate strong hydrogen bonds having distances shorter than 2.2 Å.
 - Yellow-shaded data indicate a generally acceptable range of distances for intermediate hydrogen bonds, between 2.2 and 3.0 Å.
 - Green-shaded data represent OH··· π and CH··· π interaction distances shorter than 3.05 Å.
-

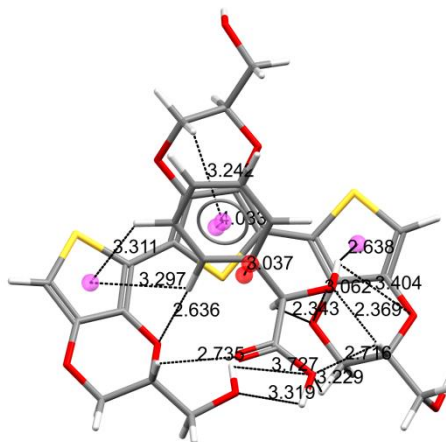
Figure S7. Structural parameters of optimized geometries.



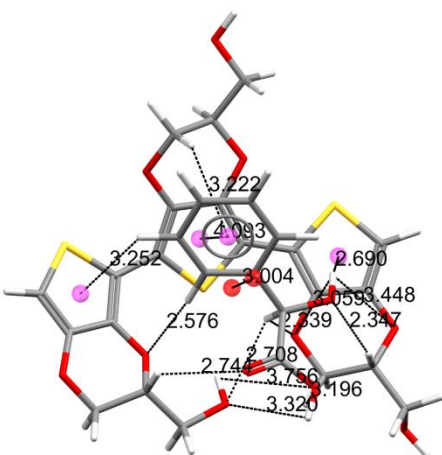
RPRM7



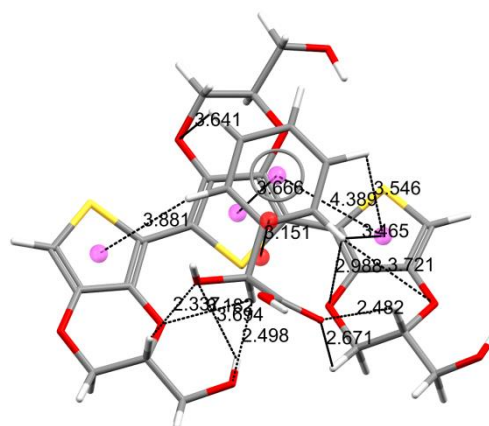
RPRM8



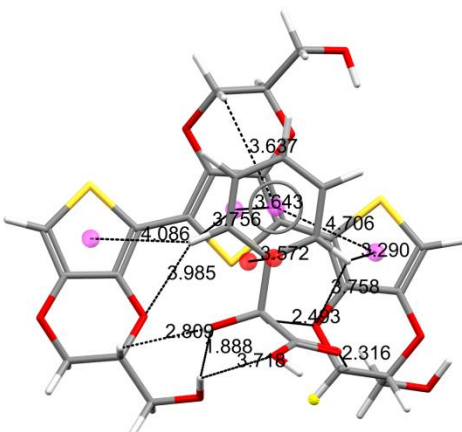
RPRM9



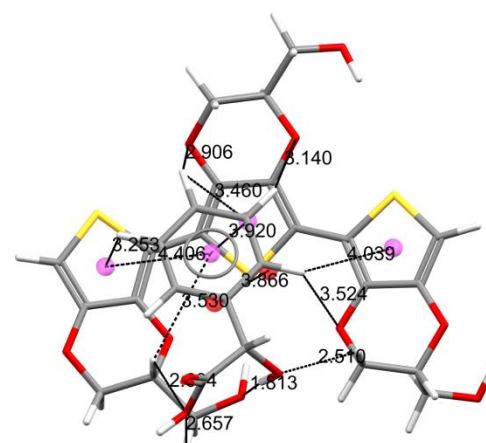
RPSM1



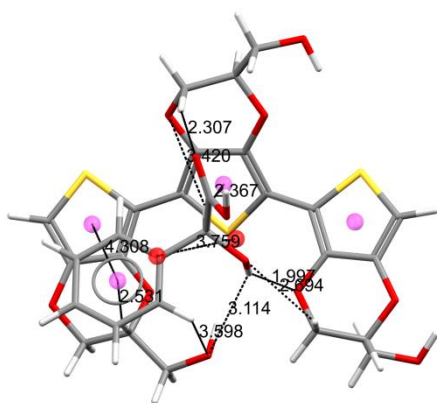
RPSM2



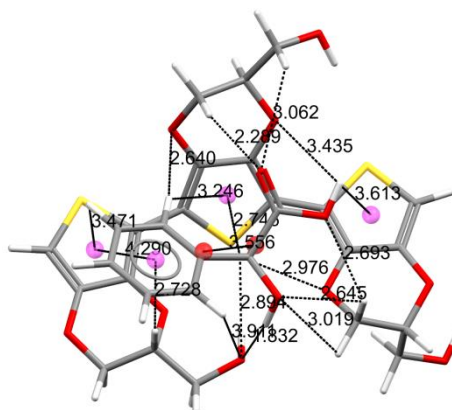
RPSM3



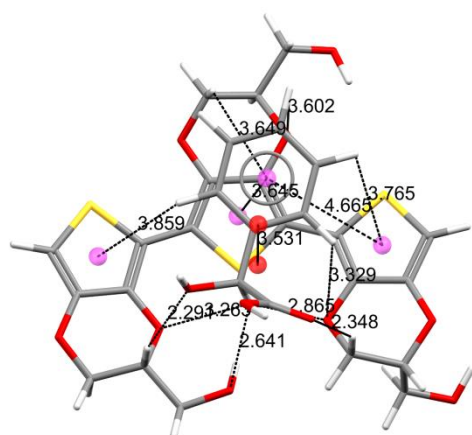
RPSM4



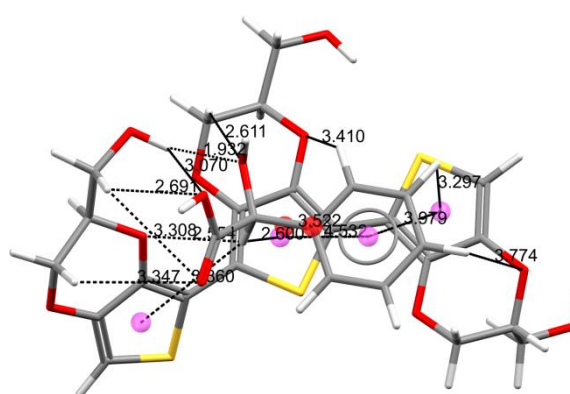
RPSM5



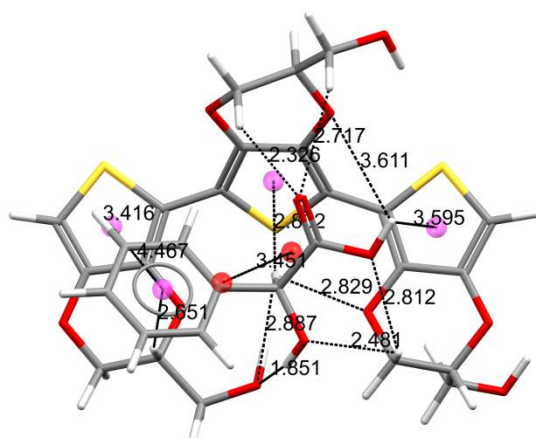
RPSM6



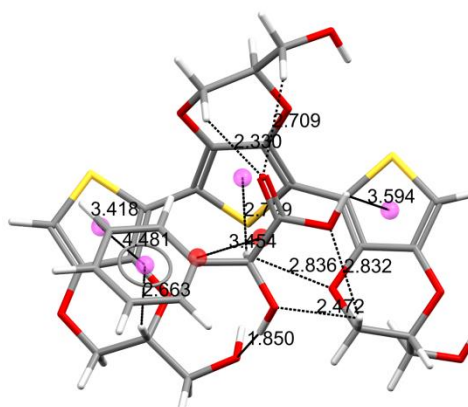
RPSM7



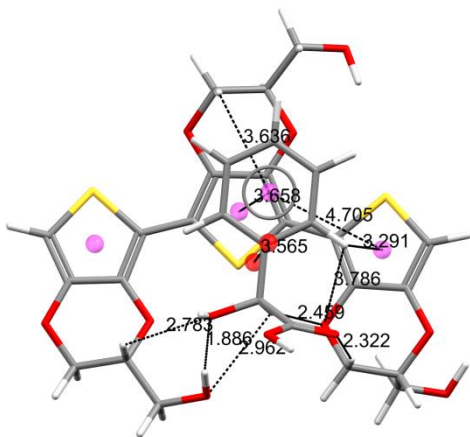
RPSM8



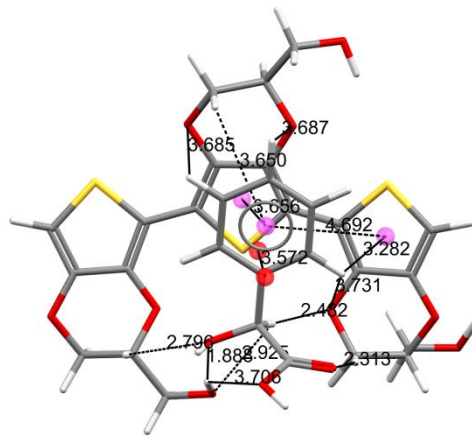
RPSM9



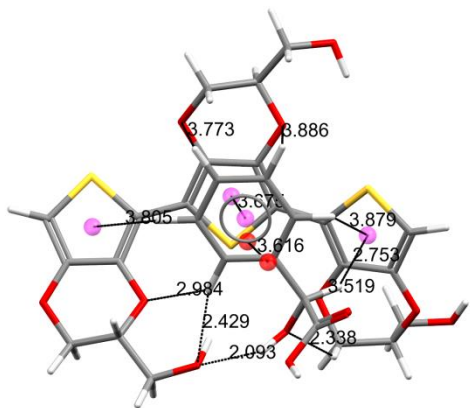
RPSM10



RPSM11



RPSM12



References

- 1 Y. Shao, Z. Gan, E. Epifanovsky, A. T. B. Gilbert, M. Wormit, J. Kussmann, A. W. Lange, A. Behn, J. Deng, X. Feng, D. Ghosh, M. Goldey, P. R. Horn, L. D. Jacobson, I. Kaliman, R. Z. Khaliullin, T. Kuś, A. Landau, J. Liu, E. I. Proynov, Y. M. Rhee, R. M. Richard, M. A. Rohrdanz, R. P. Steele, E. J. Sundstrom, H. L. Woodcock, P. M. Zimmerman, D. Zuev, B. Albrecht, E. Alguire, B. Austin, G. J. O. Beran, Y. A. Bernard, E. Berquist, K. Brandhorst, K. B. Bravaya, S. T. Brown, D. Casanova, C.-M. Chang, Y. Chen, S. H. Chien, K. D. Closser, D. L. Crittenden, M. Diedenhofen, R. A. DiStasio, H. Do, A. D. Dutoi, R. G. Edgar, S. Fatehi, L. Fusti-Molnar, A. Ghysels, A. Golubeva-Zadorozhnaya, J. Gomes, M. W. D. Hanson-Heine, P. H. P. Harbach, A. W. Hauser, E. G. Hohenstein, Z. C. Holden, T.-C. Jagau, H. Ji, B. Kaduk, K. Khistyayev, J. Kim, J. Kim, R. A. King, P. Klunzinger, D. Kosenkov, T. Kowalczyk, C. M. Krauter, K. U. Lao, A. D. Laurent, K. V. Lawler, S. V. Levchenko, C. Y. Lin, F. Liu, E. Livshits, R. C. Lochan, A. Luenser, P. Manohar, S. F. Manzer, S.-P. Mao, N. Mardirossian, A. V. Marenich, S. A. Maurer, N. J. Mayhall, E. Neuscamman, C. M. Oana, R. Olivares-Amaya, D. P. O'Neill, J. A. Parkhill, T. M. Perrine, R. Peverati, A. Prociuk, D. R. Rehn, E. Rosta, N. J. Russ, S. M. Sharada, S. Sharma, D. W. Small, A. Sodt, T. Stein, D. Stück, Y.-C. Su, A. J. W. Thom, T. Tsuchimochi, V. Vanovschi, L. Vogt, O. Vydrov, T. Wang, M. A. Watson, J. Wenzel, A. White, C. F. Williams, J. Yang, S. Yeganeh, S. R. Yost, Z.-Q. You, I. Y. Zhang, X. Zhang, Y. Zhao, B. R. Brooks, G. K. L. Chan, D. M. Chipman, C. J. Cramer, W. A. Goddard, M. S. Gordon, W. J. Hehre, A. Klamt, H. F. Schaefer, M. W. Schmidt, C. D. Sherrill, D. G. Truhlar, A. Warshel, X. Xu, A. Aspuru-Guzik, R. Baer, A. T. Bell, N. A. Besley, J.-D. Chai, A. Dreuw, B. D. Dunietz, T. R. Furlani, S. R. Gwaltney, C.-P. Hsu, Y. Jung, J. Kong, D. S. Lambrecht, W. Liang, C. Ochsenfeld, V. A. Rassolov, L. V. Slipchenko, J. E. Subotnik, T. Van Voorhis, J. M. Herbert, A. I. Krylov, P. M. W. Gill and M. Head-Gordon, *Molecular Physics*, 2015, **113**, 184-215.
- 2 Y. S. Lin, G. D. Li, S. P. Mao and J. D. Chai, *J. Chem. Theory Comput.*, 2013, **9**, 263-272.
- 3 Mercury 3.8: visualization and analysis of crystal structures. C. F. Macrae, P. R. Edgington, P. McCabe, E. Pidcock, G. P. Shields, R. Taylor, M. Towler and J. van de Streek, *J. Appl. Cryst.*, 2006, **39**, 453-457, DOI: 10.1107/S002188980600731X.

^1H and ^{13}C NMR Spectra

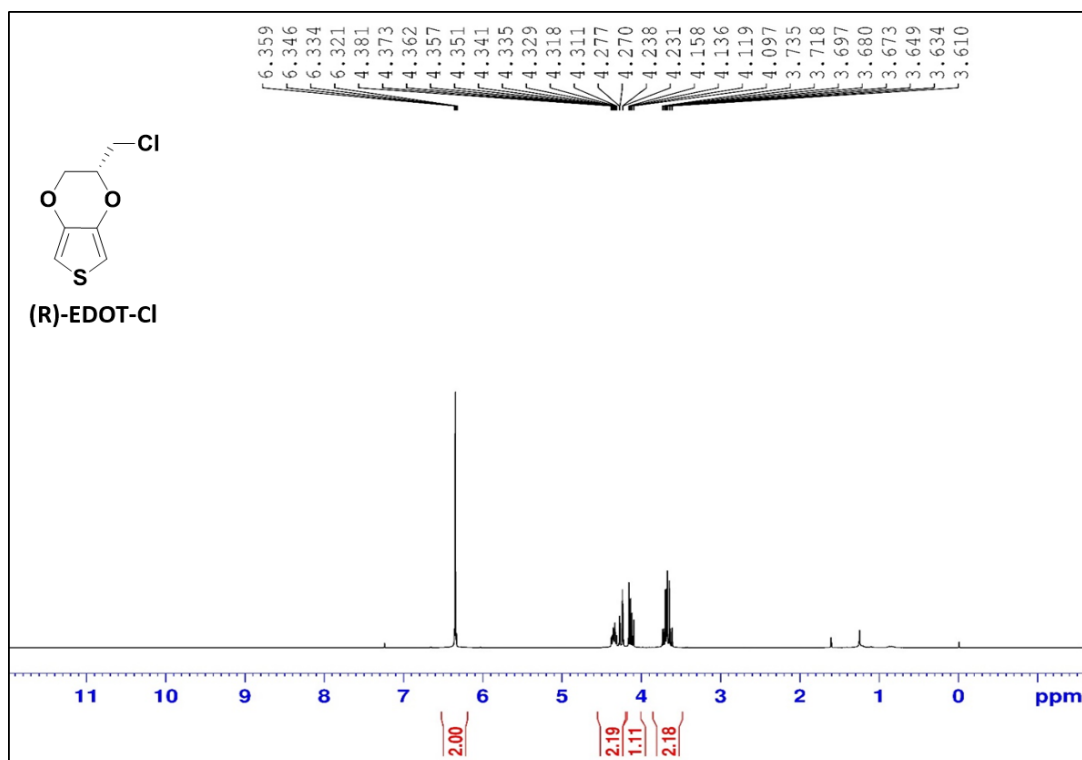


Figure S8. ^1H NMR spectrum of (R)-EDOT-Cl (400 MHz, CDCl_3).

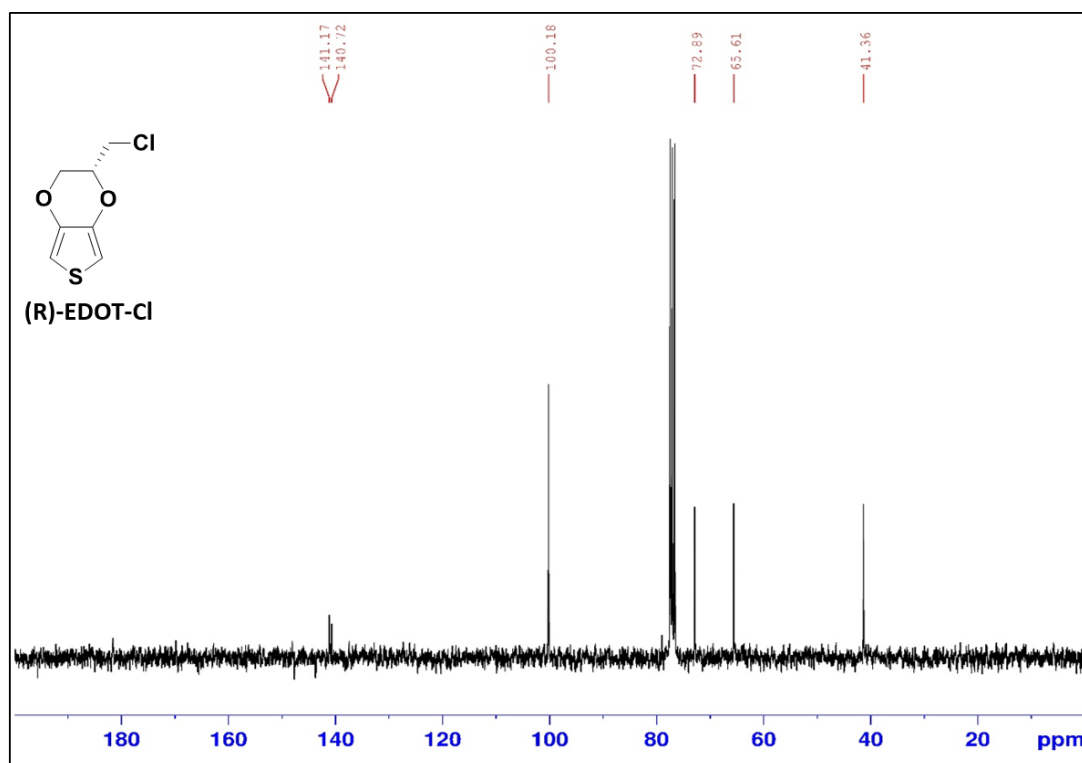


Figure S9. ^{13}C NMR spectrum of (R)-EDOT-Cl (100 MHz, CDCl_3).

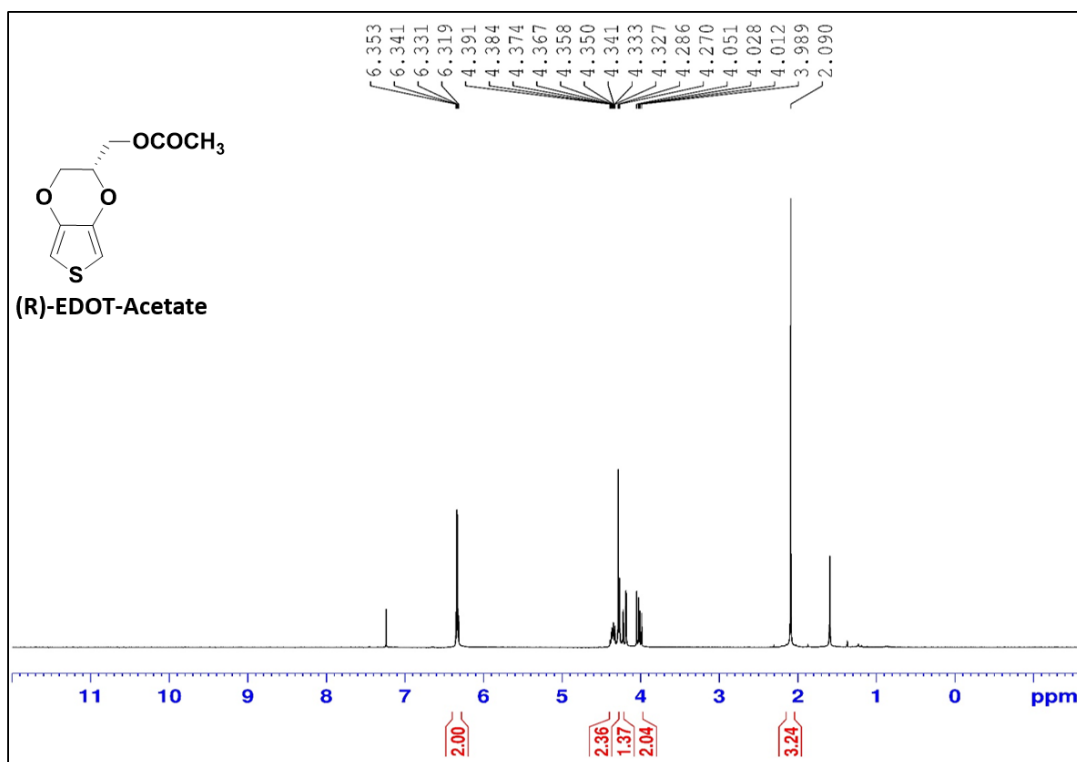


Figure S10. ¹H NMR spectrum of (*R*)-EDOT-Acetate (400 MHz, CDCl₃).

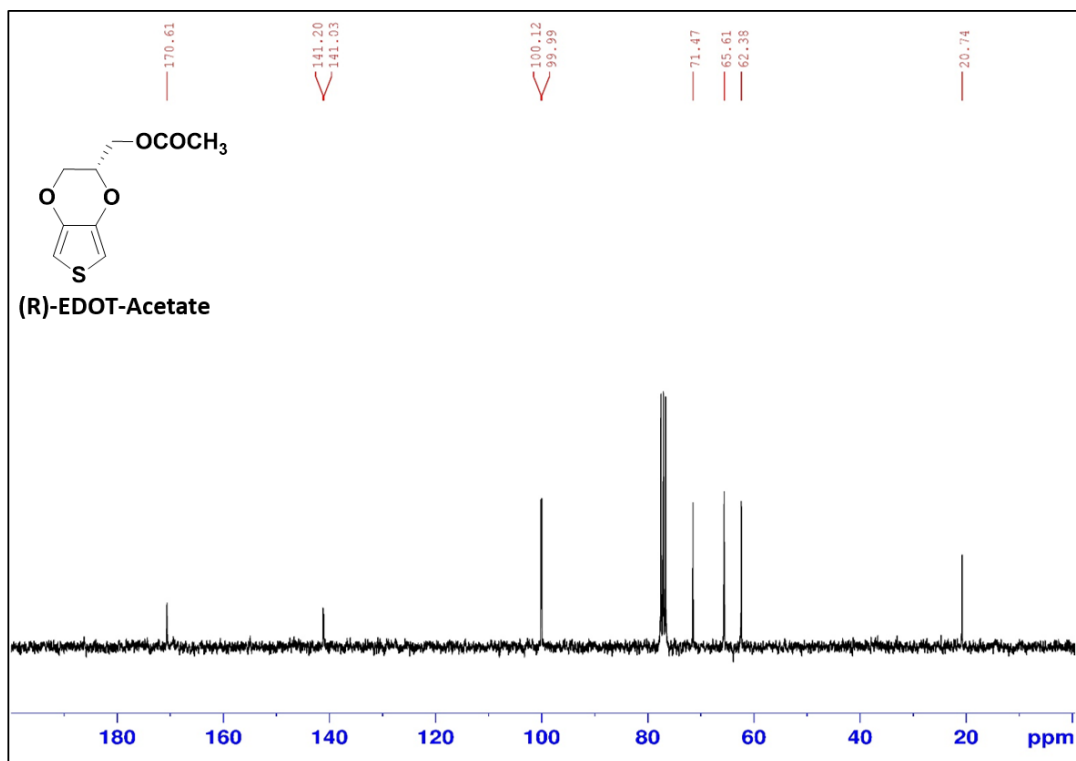


Figure S11. ¹³C NMR spectrum of (*R*)-EDOT-Acetate (100 MHz, CDCl₃).

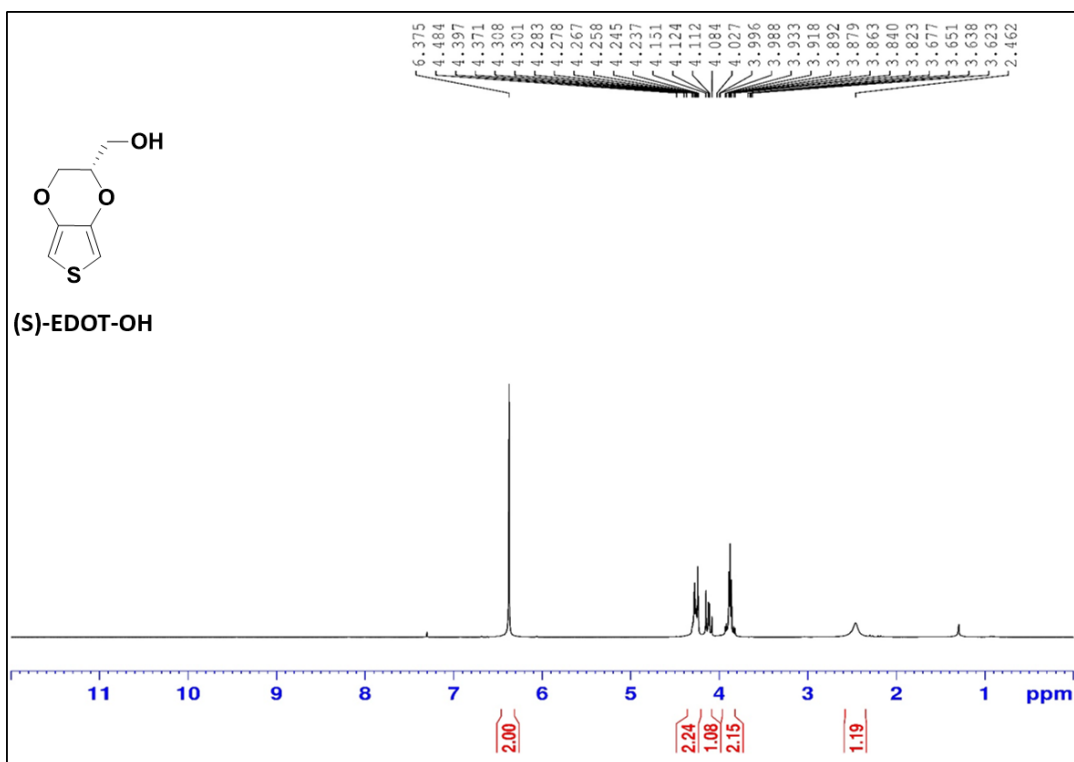


Figure S12. ^1H NMR spectrum of (*S*)-EDOT-OH (400 MHz, CDCl_3).

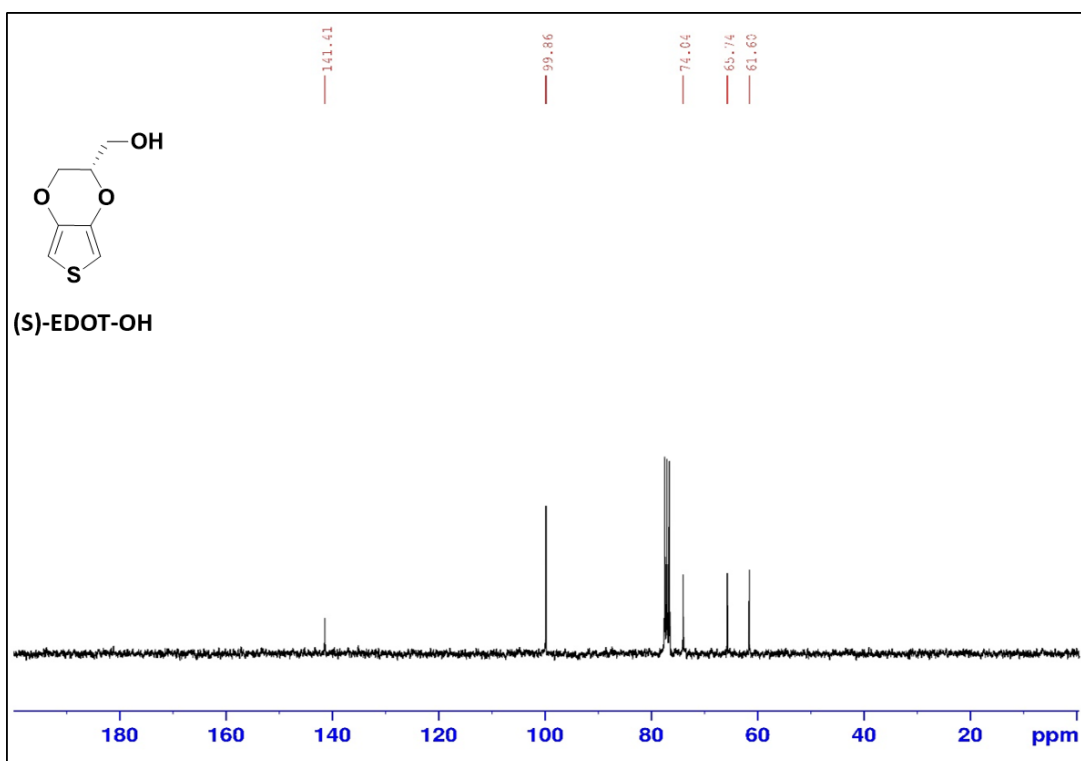


Figure S13. ^{13}C NMR spectrum of (*S*)-EDOT-OH (100 MHz, CDCl_3).

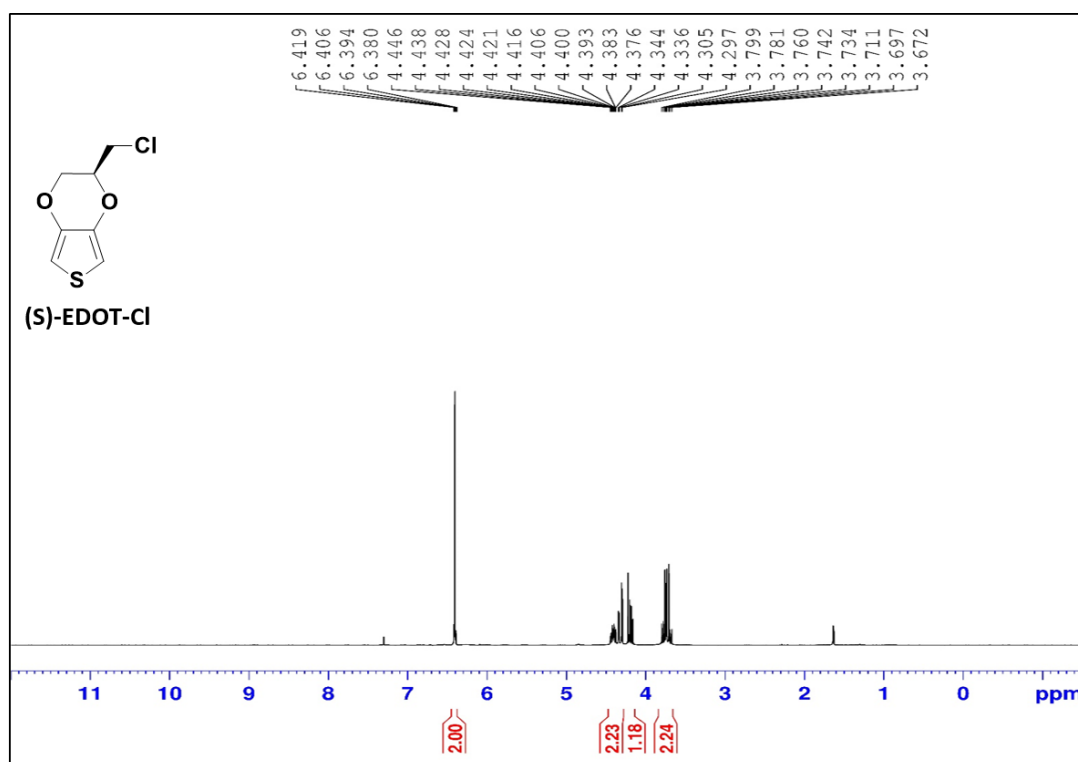


Figure S14. ^1H NMR spectrum of (*S*)-EDOT-Cl (400 MHz, CDCl_3).

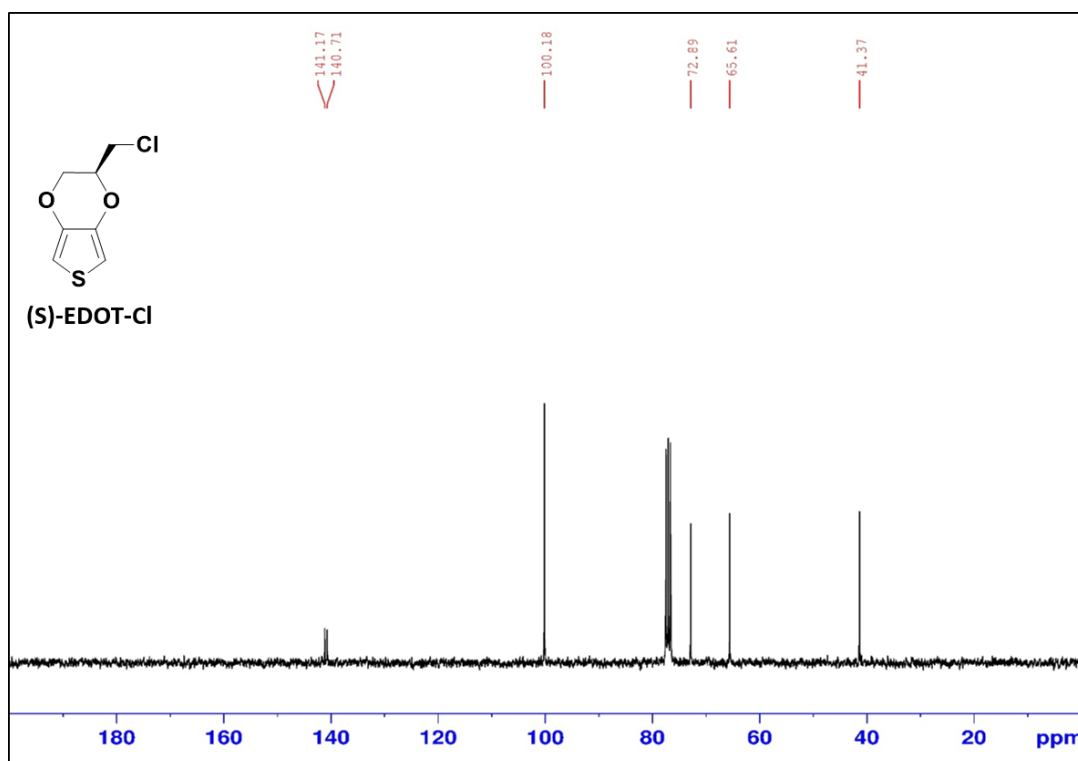


Figure S15. ^{13}C NMR spectrum of (*S*)-EDOT-Cl (100 MHz, CDCl_3).

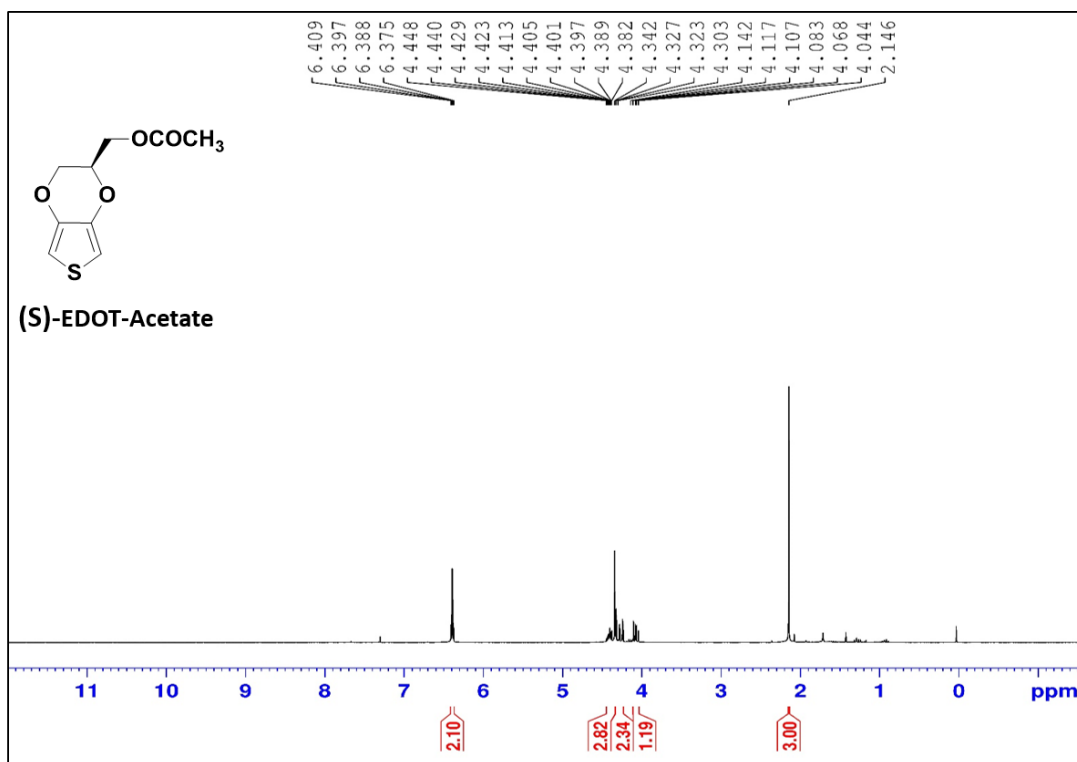


Figure S16. ^1H NMR spectrum of (*S*)-EDOT-Acetate (400 MHz, CDCl_3).

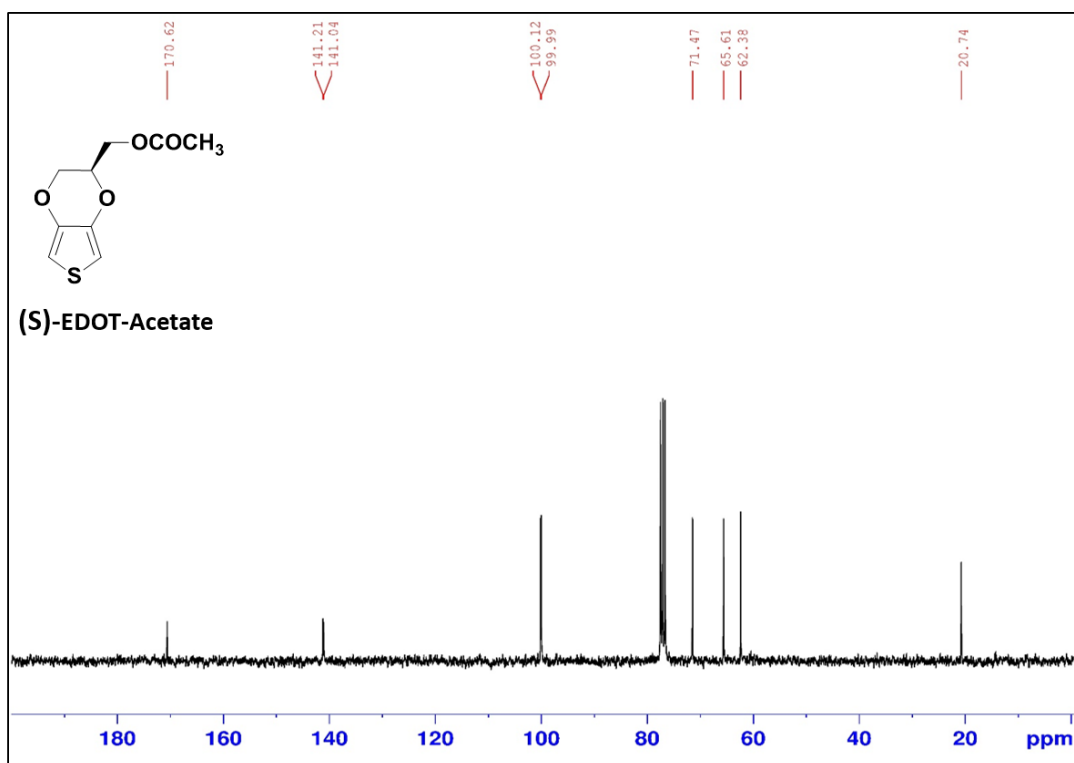


Figure S17. ^{13}C NMR spectrum of (*S*)-EDOT-Acetate (100 MHz, CDCl_3).

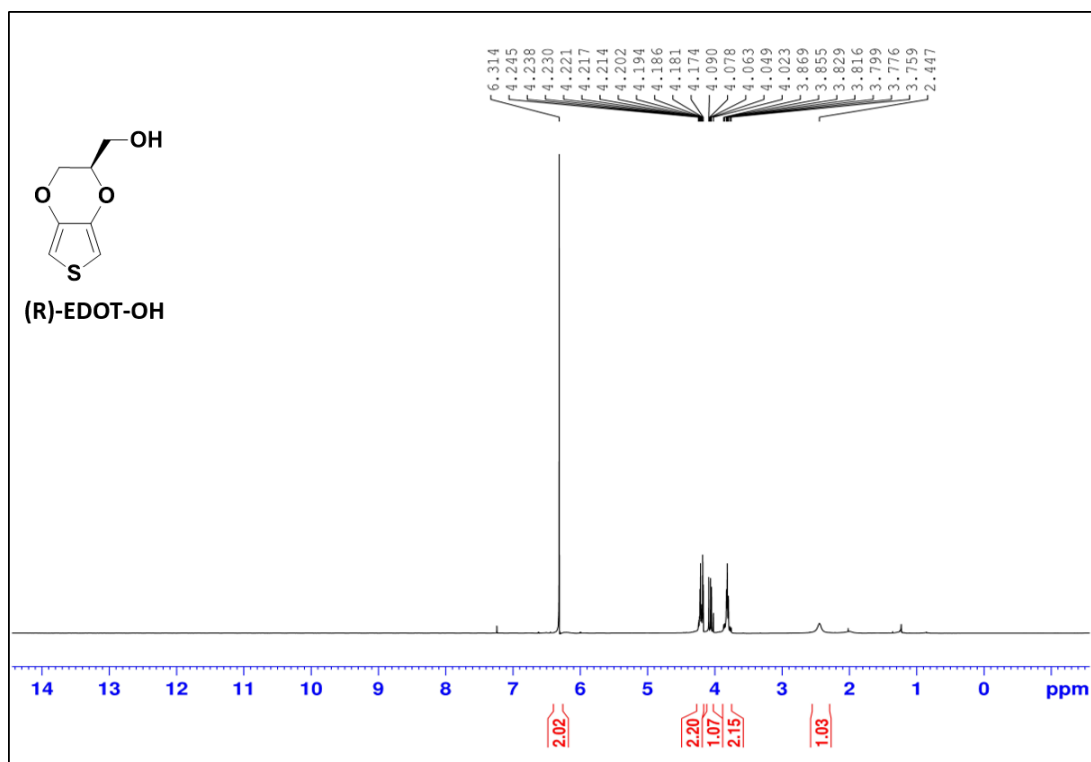


Figure S18. ¹H NMR spectrum of (R)-EDOT-OH (100 MHz, CDCl₃).

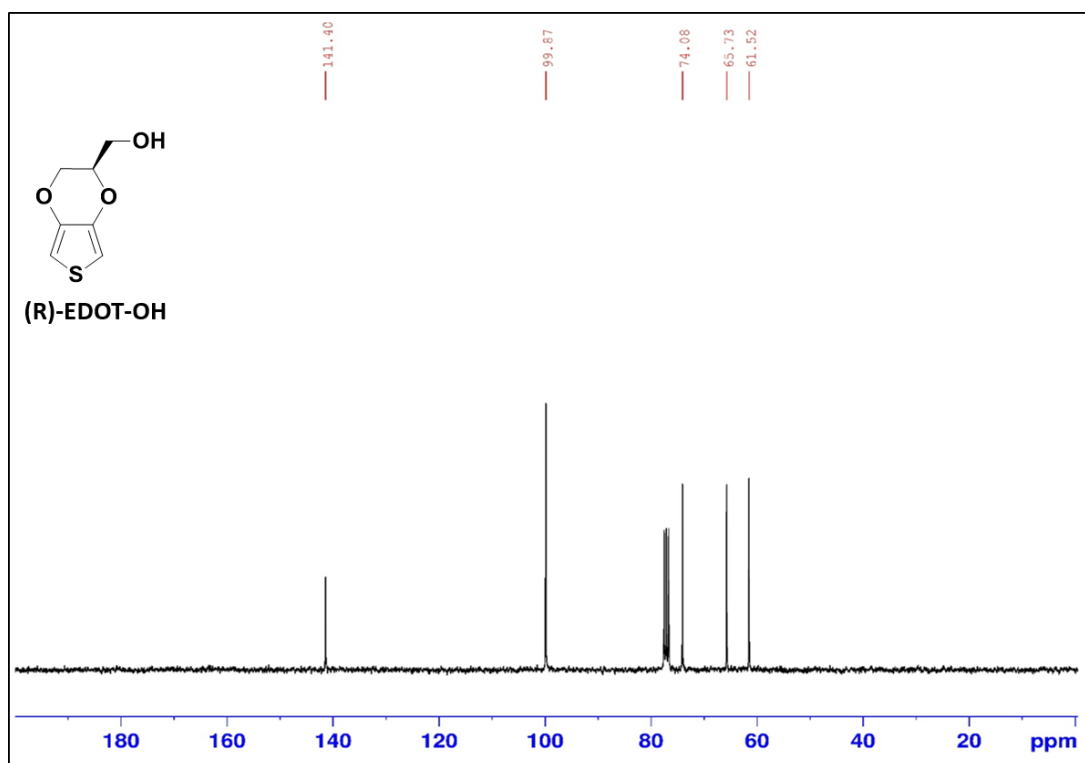


Figure S19. ¹³C NMR spectrum of (R)-EDOT-OH (100 MHz, CDCl₃).